# Super-resolution displacement mapping of unbound single molecules reveals nanoscale heterogeneities in intracellular diffusivity

Limin Xiang[‖], Kun Chen[‖], Rui Yan, Wan Li, Ke Xu*

Department of Chemistry, University of California, Berkeley, CA 94720

Chan Zuckerberg Biohub, San Francisco, CA 94158

[‖]These authors contributed equally

*Correspondence to: xuk@berkeley.edu

**Abstract**: Intracellular diffusion underlies vital processes of the cell. However, it remains difficult to elucidate how an average-sized protein diffuses in the cell with good spatial resolution and sensitivity. Here we report single-molecule displacement/diffusivity mapping (SM*d*M), a super-resolution strategy that enables the nanoscale mapping of intracellular diffusivity through the local statistics of instantaneous displacements of freely diffusing single molecules. We thus show that diffusion in the cytoplasm and in the nucleus to both be spatially heterogeneous at the nanoscale, and such variations in local diffusivity correlate strongly with the ultrastructure of the actin cytoskeleton and the chromosome, respectively. Moreover, we identify the net charge of the diffuser as a key determinant of diffusion rate: intriguingly, the possession of positive, but not negative, net charges significantly impedes diffusion, and the exact degree of slowdown is determined by the specific subcellular environments.

**Main Text:** The magic of life occurs when the right molecules meet. Whereas active transport provides an organized, yet costly means to move things around inside the eukaryotic cell, passive diffusion offers a mechanism for molecules to mix "for free". It, however, remains difficult to map out how an average-sized protein diffuses in the live cell with good spatial resolution and sensitivity. Does diffusivity contain local structures, and if so, how are they modulated by the local intracellular structures and microenvironments, as well as by the physical properties of the diffuser itself?

Although fluorescence probes have been developed to visualize intracellular parameters and processes as viscosity, macromolecular crowding, and protein-folding dynamics

(Ebbinghaus *et al.* 2010; Wirth and Gruebele 2013; Yang *et al.* 2014; Boersma *et al.* 2015; Rivas and Minton 2016), they do not directly address diffusivity. Photobleaching and photoactivation-based techniques (Lippincott-Schwartz *et al.* 2001; Ishikawa-Ankerhold *et al.* 2012) enable single-location diffusion measurements, but are unamicable to spatial mapping. Correlation-based methods (Digman and Gratton 2011; Ries and Schwille 2012; Machan and Wohland 2014) infer diffusivity from spatiotemporal fluctuations of fluorescence intensity, but are sensitive to experimental conditions (Enderlein *et al.* 2005; Ries and Schwille 2012) and achieve limited resolution and sensitivity in live cells.

Single-molecule tracking (SMT) has been successful in revealing cellular dynamics, in particular for membrane- and chromosome-bound molecules and for the confined volumes of bacteria (Manley *et al.* 2008; Kusumi *et al.* 2014; Cognet *et al.* 2014; Manzo and Garcia-Parajo 2015; Elf and Barkefors 2019). However, it remains difficult to address the more general cases of how unbound, freely diffusing molecules move inside a eukaryotic cell. To record a reasonably large area, modern high-sensitivity cameras often limit time resolution to ~10 ms (~100 frames per second). For an average-sized protein with an intracellular diffusion coefficient $D$ of ~20-30 $\mu m^2/s$ (Milo and Phillips 2016; Lippincott-Schwartz *et al.* 2001), this frame time gives rise to ~700 nm of diffusion in each dimension, hence severe motion-blur. Although stroboscopic illumination (Elf *et al.* 2007; English *et al.* 2011) overcomes motion-blur, tracking between frames remains difficult: with ~700 nm axial displacement, a molecule initially in focus readily diffuses out of the focal range (~±400 nm for a high-NA objective) in the subsequent frame (see below).

We develop a strategy to determine the nanoscale displacements of freely diffusing single molecules in short (~1 ms) time windows through the application of a pair of closely timed excitation pulses. By repeating such pulse pairs for $\sim 10^4$ times and locally accumulating the resultant single-molecule displacements, we construct super-resolution maps of diffusion rate, and hence uncover nanoscale diffusivity heterogeneities in live cells. We name this strategy single-molecule displacement/diffusivity mapping (SM*d*M), a tribute to single-molecule localization microscopy (SMLM), which generates super-resolution images by accumulating single-molecule locations (Rust *et al.* 2006; Betzig *et al.* 2006).

Whereas in SMT, each given molecule is tracked over many frames as it randomly visits different locations to enable trajectory-fitting (Kusumi *et al.* 2014; Cognet *et al.* 2014; Manzo and Garcia-Parajo 2015), SM*d*M flips the question and evaluates, for each fixed location, how different single molecules travel locally. This location-centered approach is naturally powerful for quantifying spatial heterogeneity. By removing the need to track long trajectories, SM*d*M also relaxes the requirement (Kusumi *et al.* 2014; Cognet *et al.* 2014; Manzo and Garcia-Parajo 2015) of highly photostable fluorophores. We thus focus experiments on mEos3.2, a monomeric photoswitchable fluorescent protein (FP) commonly used in SMLM (Zhang *et al.* 2012).

We expressed free mEos3.2 in the cytoplasm of mammalian cells. Along with a short cloning-site sequence, the expressed protein (mEos3.2-C1; see Methods) contained 252 amino acids (AA) (~28 kDa), close to the medium size of human proteins [248 AA by abundance (Milo and Phillips 2016)]. Under typical SMLM conditions, a 561 nm laser illuminated several micrometers into the coverslip-adhered live cells to excite a small fraction of the mEos3.2 molecules that were photoswitched to the "red" state by a weak 405 nm laser (Betzig *et al.* 2006; Manley *et al.* 2008). As expected, at a 109 Hz framerate (camera frame time $T = 9.16$ ms), freely diffusing single mEos3.2 molecules appeared blurry (Fig. 1A). The application of stroboscopic illumination (Elf *et al.* 2007; English *et al.* 2011), in which excitation pulses $\tau = 500$ µs in duration were synchronized to the center of each camera frame, provided clear single-molecule images (Fig. 1B). However, in the succeeding frame, after the frame time of $T = 9.16$ ms, molecules detected in the first frame already diffused out of the focal range and so could not be tracked (Fig. 1B).

To overcome this issue, we reduced the temporal separation between the pair of captured images by placing two excitation pulses towards the end of the first frame and the beginning of the second frame, respectively (Fig. 1C). Thus, at a $\Delta t = 1$ ms center-to-center separation between the two pulses, the molecules detected in the first frame (due to the first pulse) had only traveled moderately (to stay within focus) at the time of the second pulse (captured in the second frame) (Fig. 1C). Comparing the super-localized positions of the molecules in the two frames thus yielded their nanoscale displacements ($d$) in the $\Delta t = 1$ ms time window.

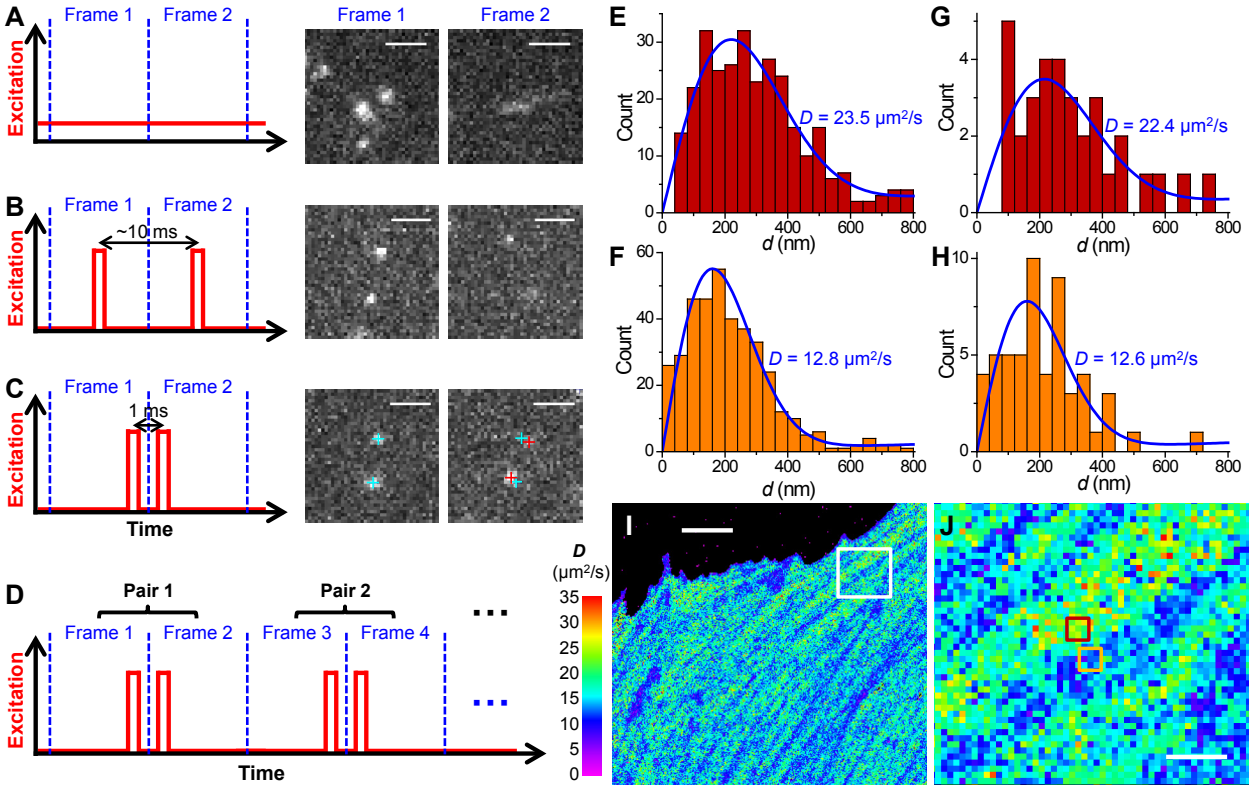


**Fig. 1. Super-resolution displacement mapping of single mEos3.2 molecules freely diffusing in the cytoplasm of live mammalian cells.** (A) Conventional imaging with continuous laser illumination and a recording framerate of 109 Hz. (B) Stroboscopic illumination, with excitation pulses $\tau$ = 500 μs in duration synchronized to the center of each camera frame. (C) Placing two excitation pulses towards the end of the first frame and the beginning of the second frame, respectively, so that the center-to-center time separation between the two recorded images is reduced to 1 ms. Cyan and red crosses mark the super-localized positions of two detected molecules in Frame 1 and Frame 2, respectively. (D) Such paired frames are repeated ~$10^4$ times to enable statistics. (E,F) Distribution of $d$ for two 300×300 nm$^2$ areas [red and orange boxes in (J)]. (G,H) Distribution of $d$ for two 100×100 nm$^2$ areas at the centers of the areas for (E,F), respectively. Blue lines in (E-H) are MLE results using eqn. 2 in Methods, with corresponding $D$ values labeled in each figure. (I,J) Map of intracellular diffusivity constructed through MLE of the $d$ distribution in every 100×100 nm$^2$ spatial bin. (J) is a zoom-in of the white box in (I). Scale bars: 2 μm (A-C), 5 μm (I), 1 μm (J).

We next repeated recording ~$10^4$ pairs of frames for statistics (Fig. 1D). The temporal proximity of the paired excitation pulses ($\Delta t$) left ample time between the unpaired pulses ($2T-\Delta t$) for different molecules to diffuse into the focal range as independent reporters of local diffusivity. The resultant, accumulated $d$ values were spatially binned to evaluate local $D$. At a

300×300 nm$^2$ bin size (Figs. 1EF), the distribution of *d* in each bin was well fitted by a modified two-dimensional random-walk model (Methods) through maximum likelihood estimation (MLE). Reducing the bin size to 100×100 nm$^2$ led to increased statistical uncertainties for each bin, but MLE still yielded reasonable results (Figs. 1GH). We further demonstrated the robustness of our fitting model for increased single-molecule density (Fig. S1). Color-plotting the *D* values obtained by individually performing MLE for each 100×100 nm$^2$ bin thus rendered a super-resolution map of local *D* across the full view (Figs. 1IJ).

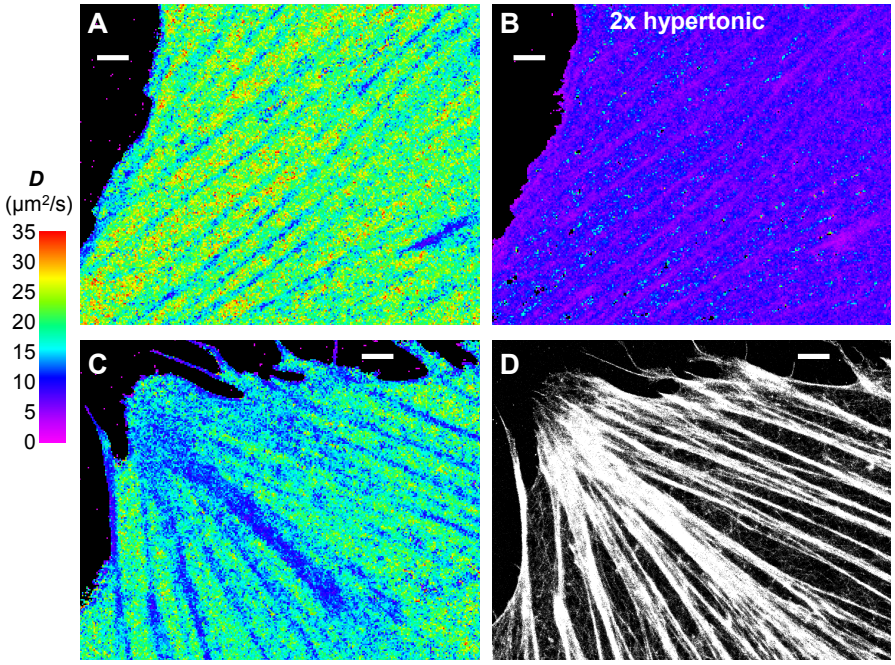


**Fig. 2. Diffusivity in the mammalian cytoplasm is spatially heterogeneous at the nanoscale due to the actin cytoskeleton.** (A) SM*d*M diffusivity map of free mEos3.2 molecules in the cytoplasm of a live PtK2 cell. (B) The same cell in a 2× hyperosmotic medium. (C,D) Correlated SM*d*M diffusivity map of mEos3.2 in another live PtK2 cell (C), vs. SMLM image of AF647 phalloidin-labeled actin in the fixed cell (D). Scale bars: 2 μm.

For mEos3.2 molecules freely diffusing in the cytoplasm of live mammalian cells, we observed typical *D* of 20-25 μm$^2$/s for the high-*D* regions (Figs. 1IJ, 2AC, and S2), comparable to previous, spatially unresolved results of FPs (Lippincott-Schwartz *et al.* 2001; Milo and Phillips 2016). Treating the cells with a 2× hyperosmotic medium led to substantially reduced *D* down to ~8 μm$^2$/s for the high-*D* regions (Fig. 2B), consistent with increased macromolecular crowding owning to water loss (Boersma *et al.* 2015).

Our ability to map local *D* throughout the cell revealed substantial diffusivity heterogeneities at the nanoscale. For the flat, spread parts of cells, SM*d*M *D* maps often showed continuous, linear features characterized by markedly reduced *D* values down to ~10 $\mu m^2/s$ (Figs. 2AC and S2). The distinct linear structures are reminiscent of the actin cytoskeleton, which often form linear bundles as stress fibers (Tojkander *et al.* 2012). Indeed, SMLM of the Alexa Fluor 647 (AF647) phalloidin-labeled actin in the fixed cell showed good correspondences between actin bundles and the SM*d*M-revealed low-*D* regions in the live cell (Figs. 2CD and S2). Previous work suggests that at the whole cell level, the actin cytoskeleton impedes intracellular diffusion (Potma *et al.* 2001; Baum *et al.* 2014). Here, SM*d*M resolved nanoscale heterogeneity in *D*, and directly linked local decreases in *D* to the actin ultrastructure. Interestingly, a protein-folding sensor shows linear intracellular structures of elevated local melting temperature (Ebbinghaus *et al.* 2010; Wirth and Gruebele 2013), which could be consistent with macromolecular crowding effects at actin bundles, in line with the diffusion slowdown we observed.

We next examined diffusion in the nucleus. By setting the focal plane a few micrometers into the cell, we imaged at the central depths of the nuclei. SM*d*M (Fig. 3A and Fig. S3) yielded *D* of ~20 $\mu m^2/s$ for the highest-*D* regions of the nucleus (red arrows), consistent with the view that the nucleosol and cytosol share similar diffusion properties (Seksek *et al.* 1997). Meanwhile, micron-sized globule structures were noted, where the local *D* dropped drastically to ~6 $\mu m^2/s$ (white asterisk in Fig. 3A). The globule shape is reminiscent of the nucleolus, a subnuclear compartment for ribosome biogenesis (Boisvert *et al.* 2007). Our bright-field transmission images supported this assignment (Fig. S3). The observed, much-reduced *D* in the nucleolus is consistent with its high crowdedness of proteins and nucleic acids (Boisvert *et al.* 2007).

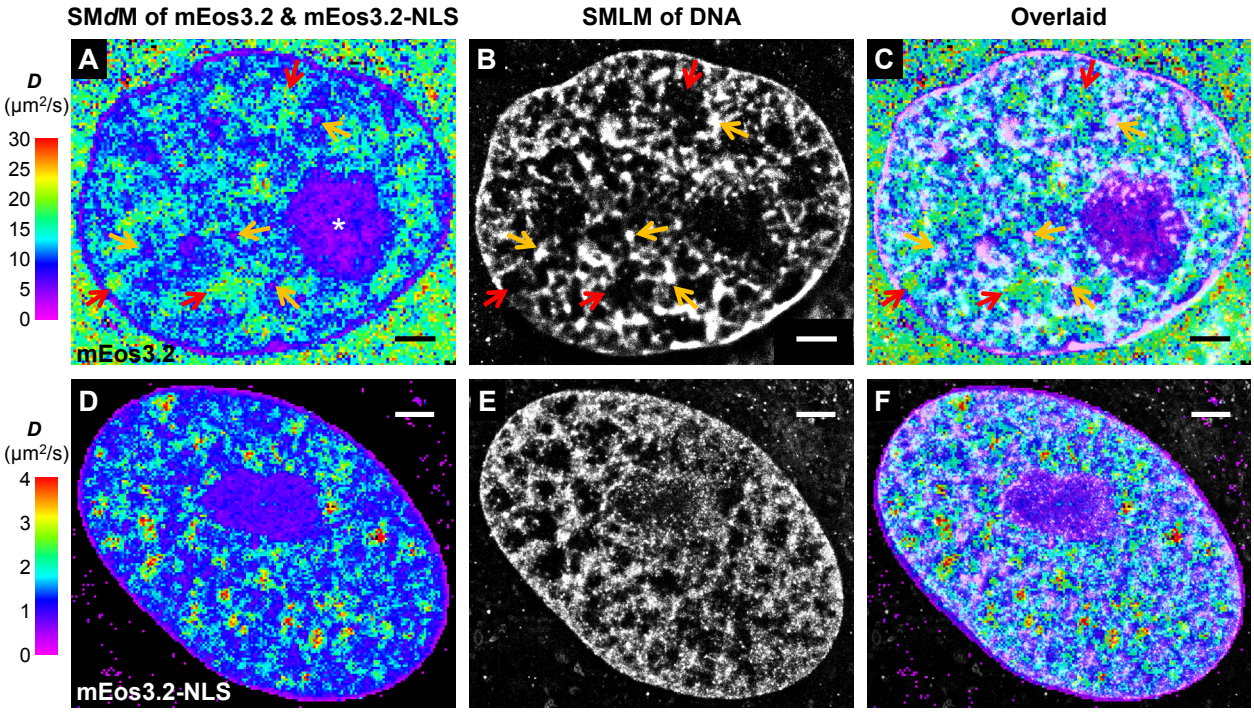


**Fig. 3. Diffusivity in the mammalian nucleus is spatially heterogeneous at the nanoscale due to the nucleolus and the chromatin.** (A) SM*d*M diffusivity map of free mEos3.2 at the central depth of the nucleus of a live PtK2 cell. (B) SMLM image of the fixed cell using the DNA stain NucSpot Live 650. (C) Overlay of (A) and (B). (D) SM*d*M diffusivity map of mEos3.2-NLS in the nucleus of a live PtK2 cell. (E) SMLM image of NucSpot-stained DNA of the fixed cell. (F) Overlay of (D) and (E). Scale bars: 2 μm.

Close examination of the SM*d*M data further revealed semi-structured, fractal-like nanoscale features of lowered $D$ (~10 μm$^2$/s), which sporadically evolved into ~200 nm sized foci of very low $D$ of ~6 μm$^2$/s (orange arrows in Fig. 3A). SMLM of the DNA ultrastructure of the fixed cell (Fig. 3B) showed a strong spatial correlation: the highest-$D$ regions in the SM*d*M map of mEos3.2 consistently matched to regions devoid of DNA (red arrows in Fig. 3A-C), whereas the low $D$ regions corresponded to DNA structures, with the slowest foci often corresponding to clusters of high local DNA density (orange arrows), a structure indicative of densely packed structures as the heterochromatin. See Fig. S3 for additional examples: the spatial patterns of diffusivity correlated well with diverse chromatin ultrastructures.

Our results above implicate chromatin crowding as a major impediment to intranuclear diffusion. Single-location fluorescence correlation spectroscopy (FCS) measurements in a previous study (Bancaud *et al.* 2009) show reduced $D$ at the chromatin and the nucleolus. In a

different study, however, FCS mapping in ~1 μm-spaced arrays finds no correlations between *D* and chromatin structures (Dross *et al.* 2009). Our correlated SM*d*M and SMLM data establish a definite association, at the nanoscale, between locally reduced *D* and the ultrastructures of the chromatin and nucleolus. Such coexistence of fast and slow diffusion domains may be functionally important, as envisioned by the chromosome-territory–interchromatin-compartment (CT-IC) model (Cremer and Cremer 2001).

We next examined what properties of the diffuser itself affect intracellular diffusion behavior, and identified electrical charge as a key determinant. This effort was driven by an unexpected observation we made when adding a nuclear localization sequence [NLS; $(DPKKKRKV)_3$] to mEos3.2: although SM*d*M maps of mEos3.2-NLS again correlated well with the SMLM-resolved DNA, the actual *D* values dropped by one order of magnitude (Fig. 3D-F). As this big drop is unlikely due to the small added size of NLS, we questioned whether the notably positive charge of the sequence played a role. Under the physiological pH of 7.4, our original mEos3.2 expression had a total charge of +2. With the NLS sequence, the net charge became +15. Consequently, we shifted the net charges of the expressed mEos3.2 protein sequences to −14, −7, 0, +7, and +14 by adding short sequences of Arg/Lys and Asp/Glu to the C-terminus (Methods).

SM*d*M showed a peculiar trend: For all subcellular environments, the two negatively charged (−14, −7) constructs (Fig. 4AB) both yielded *D* comparable to that of the neutral (0 charges) species (Fig. 4C), but slightly higher than that of the original mEos3.2-C1 construct (+2 charges) (Figs. 2, 3, and 4F). For the more positively charged protein (+7), however, markedly reduced *D*, down to half of that of the negative and neutral species, was found across all subcellular environments (Fig. 4DF). Meanwhile, extremely slow diffusion was found for the +14 charged construct: Curiously, as *D* dropped to ~0.5 $\mu m^2/s$ in the cytoplasm, notably higher values of up to ~3 $\mu m^2/s$ were retained inside the nucleus (Fig. 4E), comparable to what we initially noticed for mEos3.2-NLS (+15 charges; Fig. 3D). Together, we found that whereas a negative net charge does not significantly affect protein diffusion, the possession of positive net charges is a key factor for diffusion slowdown, and the degree of slowdown depends strongly on the specific subcellular environments (Fig. 4F).

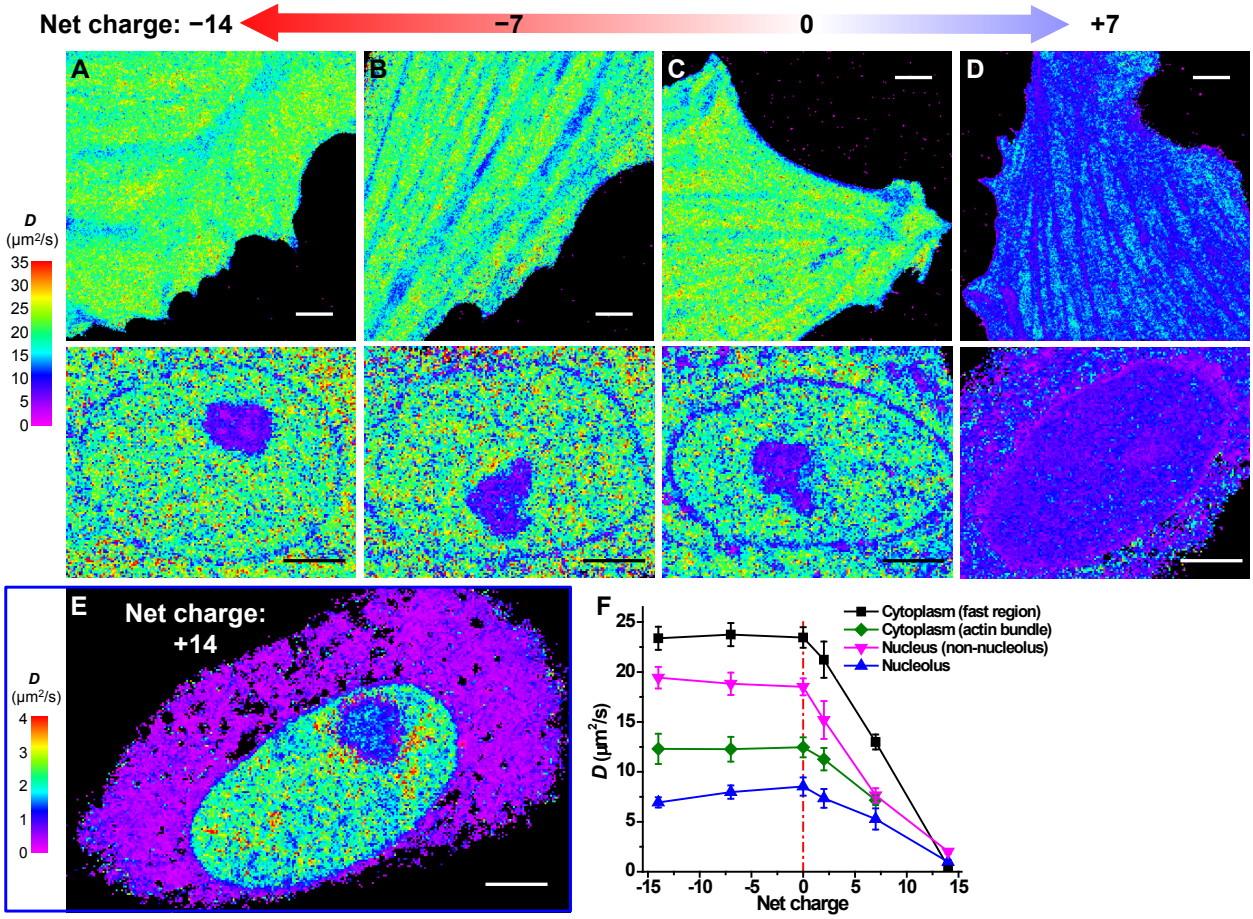


**Fig. 4. The possession of positive, but not negative, net charges is a key determinant of diffusivity in the mammalian cell.** (A-D) SM*d*M diffusivity maps of mEos3.2 constructs of −14 (A), −7 (B), 0 (C), and +7 (D) net charges expressed in PtK2 cells. The top and bottom panels show representative results in the spread parts of cells and the nuclei, respectively. (E) SM*d*M diffusivity map for the +14 charged mEos3.2 construct, on a substantially reduced *D* scale. (F) Mean *D* values for the above differently charged mEos3.2 proteins in different subcellular environments. For cytoplasm, we present the averaged *D* for fast regions with no apparent slowdown due to the actin cytoskeleton (black), as well as for the actin-bundle regions (green). The nucleus data are simply divided into nucleolus (blue) and non-nucleolus (magenta) regions. Error bars: standard deviations between different cells ($n$ > 6 cells for each data point). Scale bars in (A-E): 4 μm.

This strong dependence on positive net charges may have evaded previous attention as many FPs are highly negatively charged (*e.g.*, −7 charges for most GFP derivatives, including EGFP, ECFP, and Venus). Notably, in bacteria, a recent study (Schavemaker *et al.* 2017) has examined the diffusion of differently charged GFP proteins, and also finds that all negatively charged and neutral GFPs diffuse alike, whereas positively charged GFPs diffuse much slower, a

result ascribed to interaction with the negatively charged ribosomes. The mammalian cell, however, is a more complicated system.

Intriguingly, the mammalian cytosol contains a high (~150 mM) concertation of small cations, notably $K^+$, whereas the total concentration of small anions is disproportionally low (~15 mM) (Lodish *et al.* 2003). Charge balance thus mandates intracellular bio(macro)molecules to take the negative charges. Whereas the backbones of DNA and RNA are known as negatively charged, the net charges of proteins are less discussed (Gitlin *et al.* 2006; Smith *et al.* 2016; Schavemaker *et al.* 2017; Mu *et al.* 2017). We noticed (Table S1) that a majority of proteins in the cytoplasm of mammalian cells to be either strongly negatively charged or neutral. For instance, the most abundant cytoskeletal proteins, β-actin, α-tubulin, and vimentin, carry net charges of −12, −24, and −19, respectively, whereas the most abundant molecular chaperones, Hsp90ab1 and HspA8, have −39 and −13 net charges.

Consequently, the peculiar, asymmetric charge dependency of *D* we found (Fig. 4F) may be rooted in the asymmetric intracellular abundance of positively charged, small metal ions vs. negatively charged, large biomolecules. For intracellular diffusion, whereas a negatively charged diffuser is readily neutralized by the abundant small cations and so behaves similarly as neutral diffusers, a positively charged diffuser is not effectively screened by small ions: dynamic interactions with the negatively charged, large intracellular biomolecules substantially hinder diffusion (Fig. S4). At a fundamental level, such impediments to diffusion may, conversely, explain the above-noted preponderance of negatively charged proteins in the cell (Table S1): the cell may have evolved to agree on a negatively charged convention to minimize nonspecific interactions and diffusion slowdown, since DNA and RNA are negatively charged in the first place.

Together, we have shown how the local statistics of instantaneous displacements of unbound single molecules can unveil rich, nanoscale heterogeneities in intracellular diffusivity. Whereas here fascinating results were obtained with free FPs, we expect SM*d*M with FP-tagged proteins to be powerful in probing specific protein-protein interactions. The further integration of SM*d*M with other emerging super-resolution methods, *e.g.*, spectrally resolved SMLM (Yan *et al.* 2018), represents additional exciting possibilities.

**Acknowledgments:** We thank Seonah Moon for discussion, and Manni He and Yennie Shyu for help with preparation of the DNA constructs. This work was supported by the National Institute Of General Medical Sciences of the National Institutes of Health (DP2GM132681), the Beckman Young Investigator Program, and the Packard Fellowships for Science and Engineering. K.X. is a Chan Zuckerberg Biohub investigator.

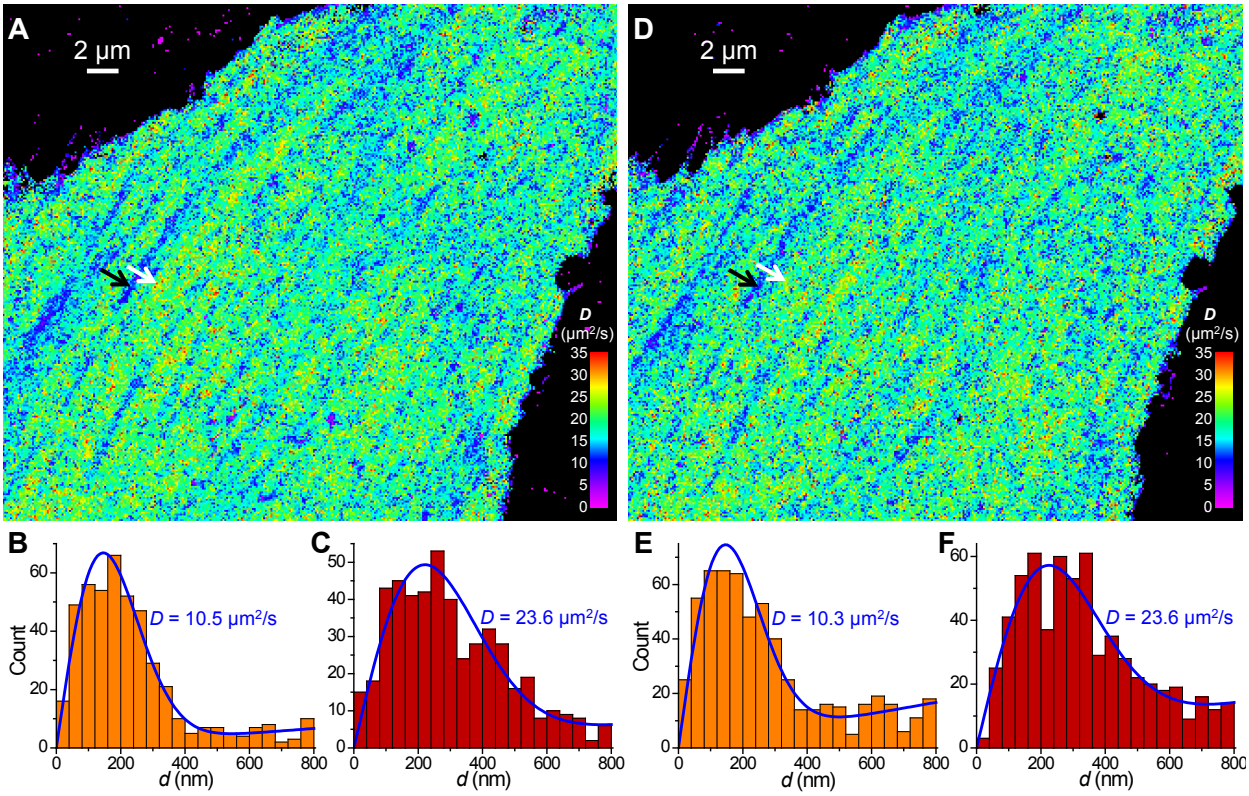


**Fig. S1. SM*d*M results at different single-molecule densities.** Free mEos3.2 was expressed in the cytoplasm of a PtK2 cell, and SM*d*M was performed on the same cell at a low single-molecule density for 60,000 pairs of pulses (A-C), or at a high single-molecule density for 30,000 pairs of pulses (D-F) by increasing the power of the photoactivation (405 nm) laser. (A) SM*d*M diffusivity map for the low single-molecule density experiment, obtained by spatially binning the single-molecule displacement *d* data onto 120×120 nm$^2$ grids, and then individually fitting the distribution of *d* in each bin to eqn. 2 through MLE. (B,C) Distribution of *d* for two 360×360 nm$^2$ areas pointed to by the black (for B) and white (for C) arrows in (A), respectively. Blue lines are MLE results using eqn. 2, with the resultant *D* values labeled in each figure. (D-F) Results of the high single-molecule density experiment: comparable *D* values are obtained with the much-reduced number of pulse pairs, despite an increased background due to single-molecule mismatch.

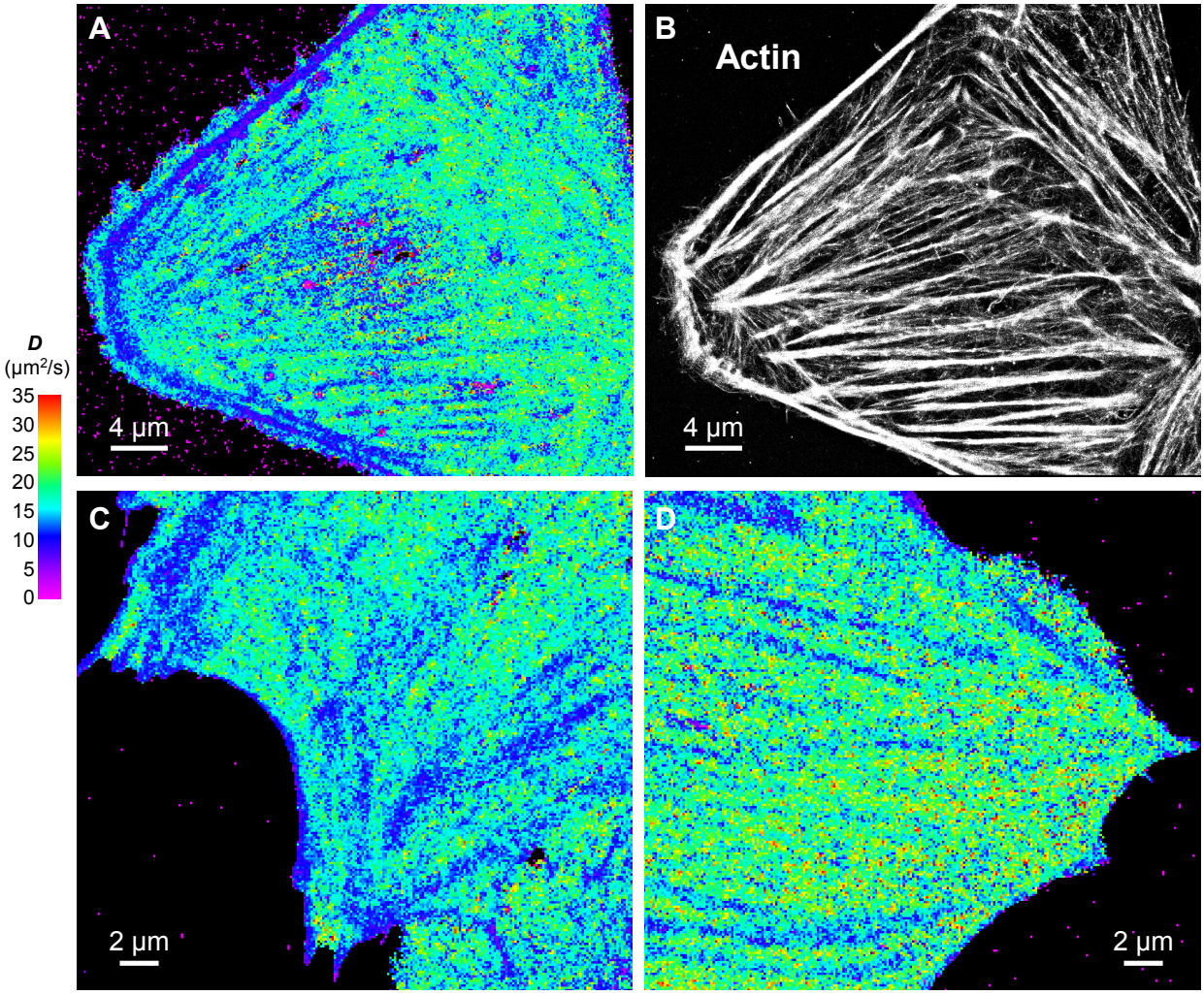


**Fig. S2. Additional SM*d*M results of free mEos3.2 in the cytoplasm of live U2OS and PtK2 cells.** (A,B) Correlated SM*d*M diffusivity map for a live U2OS cell (A) vs. SMLM image of AF647 phalloidin-labeled actin in the fixed cell (B). (C,D) Additional SM*d*M diffusivity maps for the cytoplasm of PtK2 cells.

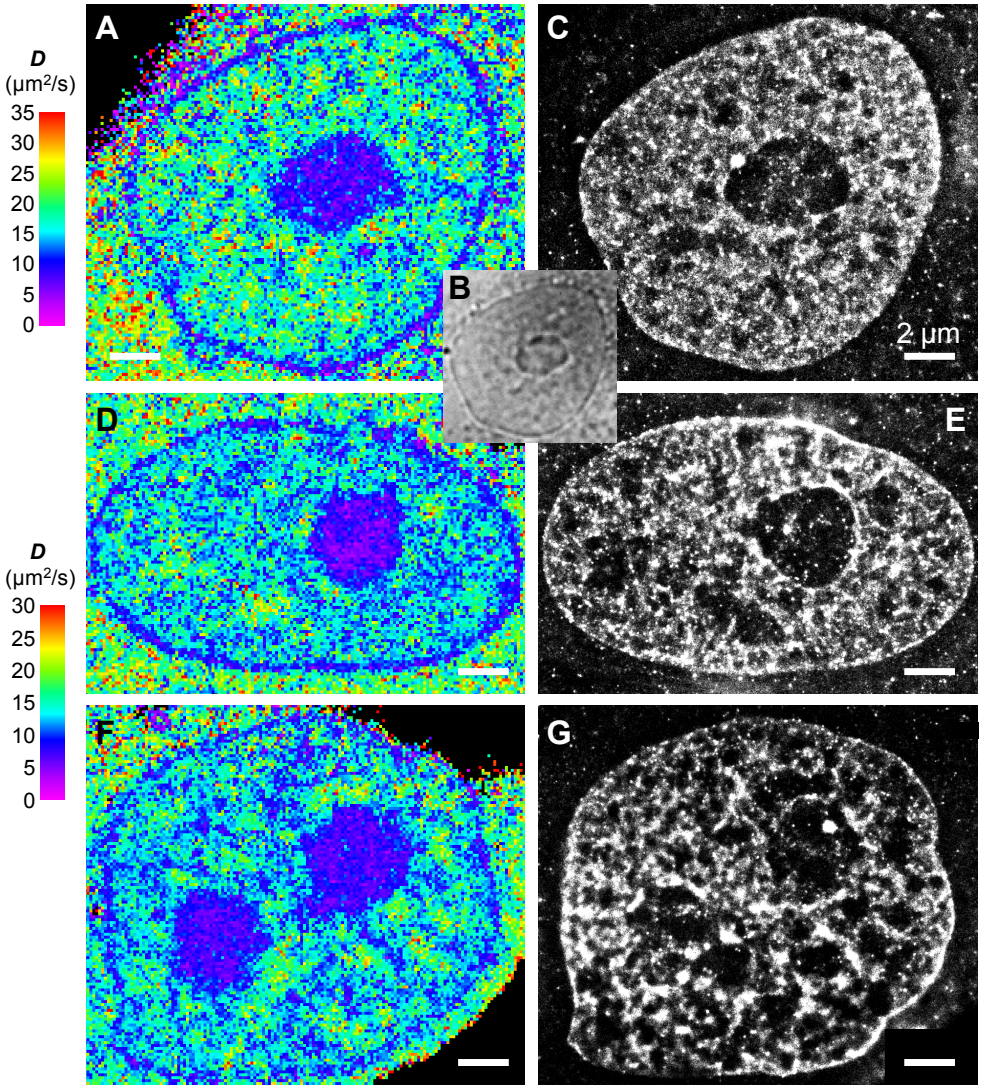


**Fig. S3. Additional SM*d*M results of free mEos3.2 in the nuclei of live PtK2 cells.** (A,D,F) SM*d*M diffusivity maps of 3 different cells. (B) Bright-field transmission image of the same view as (A), visualizing the nucleolus. (C,E,G) SMLM images of the fixed cells in (A,D,F) using the DNA stain NucSpot Live 650. We note that as the SMLM of DNA was performed after fixation and multiple washing steps, it was difficult to image at exactly the same focal plane as the live-cell SM*d*M experiment, which accounts for some of the apparent structural mismatches. Scale bars: 2 μm.

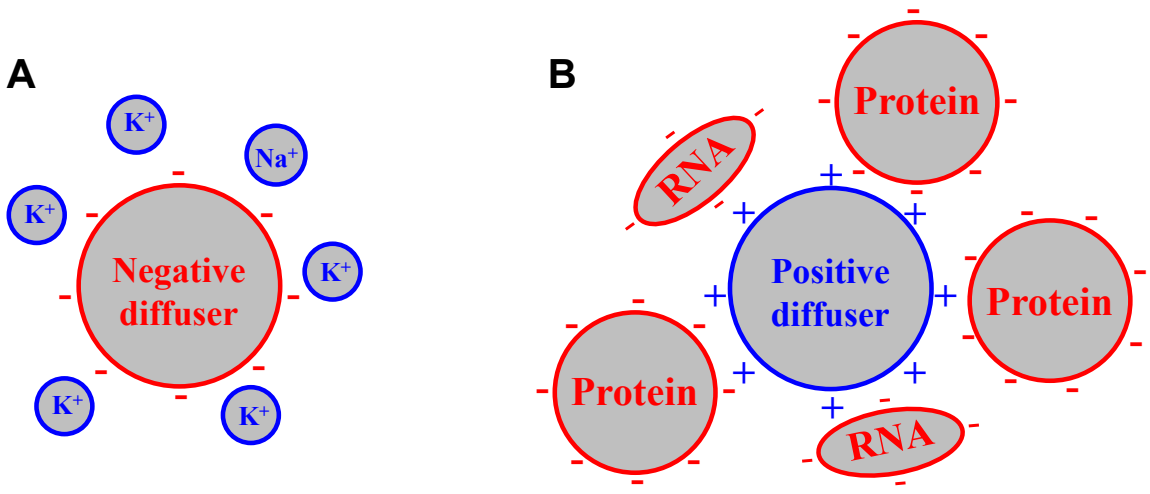


**Fig. S4. Asymmetric effects of negative and positive net charges on intracellular diffusion owing to the asymmetric intracellular abundance of positively charged, small ions vs. negatively charged, large biomolecules.** (A) A negatively charged diffuser is readily neutralized by the abundant small cations inside the cell, and so diffuses similarly as neutral counterparts. (B) A positively charged diffuser is not effectively neutralized/screened by small ions; its dynamic interactions with the negatively charged, large biomolecules insides the cell substantially hinder diffusion.

**Table S1.** List of estimated net charges for the most abundant (>0.2% of total protein mass) cytoplasmic proteins, based on the proteomics of the common U2OS cell line (Liebermeister *et al.* 2014). Protein sequences were obtained from UniProt (https://www.uniprot.org/). Net charges were estimated for pH 7.4 via Protein Calculator (http://protcalc.sourceforge.net/). For each category, proteins are listed in the order of mass abundance (% of total protein mass of the cell). This showed that most proteins in the categories of "cytoskeletal proteins", "chaperones and folding catalysts", and "others" are either strongly negatively charged (<−10) or neutral (within ±2). Half of the proteins in the "glycolysis" group are mildly (~+3) positive, possibly for their aimed interactions with the negatively charged, phosphorylated glucose metabolites, which thereby neutralizing the total charge. Three proteins in the group of "ribosome" and one in "translation factors" are strongly positively charged, but these positive charges are overcompensated by the heavily negatively charged backbone of RNA, their binding partner (Knight *et al.* 2013; Schavemaker *et al.* 2017). Earlier analysis not considering the relative abundances also suggests a majority of cytoplasmic proteins to be negatively charged (Schwartz *et al.* 2001).

**Cytoskeletal proteins & regulators**

| Name | %mass | Net charge |
|---|---|---|
| Vim | 2.7 | -18.6 |
| TubA1c | 2.2 | -22.7 |
| ActB | 2.2 | -11.7 |
| Cfl1 | 1.2 | 1.6 |
| FlnA | 0.84 | -50.8 |
| Plec | 0.83 | -76.9 |
| myh9 | 0.71 | -45.9 |
| pfn1 | 0.68 | 1.8 |
| FlnB | 0.36 | -60.9 |
| FlnC | 0.32 | -54.6 |
| TubB6 | 0.30 | -24.7 |
| LmnA | 0.29 | -2.1 |
| Myl6 | 0.28 | -14.0 |
| SptAn1 | 0.27 | -106.4 |

**Chaperones and folding catalysts**

| Name | %mass | Net charge |
|---|---|---|
| Hsp90ab1 | 2.2 | -39.3 |
| HspA8 | 2.0 | -12.8 |
| cct2 | 1.1 | -7.9 |
| PPIA | 0.97 | 0.9 |
| HspD1 | 0.89 | -5.2 |
| HspB1 | 0.60 | -2.7 |
| cct6a | 0.40 | -4.5 |
| cct5 | 0.20 | -13.6 |

**Glycolysis**

| Name | %mass | Net charge |
|---|---|---|
| Pkm2 | 3.1 | 2.4 |
| Eno1 | 2.5 | 0.0 |
| GAPDH | 2.0 | 3.6 |
| Tpi1 | 1.7 | -5.0 |
| AldOa | 1.1 | 3.2 |
| Pgk1 | 0.85 | 2.8 |
| LdhA | 0.53 | 3.2 |
| Eno3 | 0.48 | 1.1 |
| Eno2 | 0.22 | -18.0 |

**Ribosome**

| Name | %mass | Net charge |
|---|---|---|
| Rpl37a | 0.54 | 18.7 |
| Rps15a | 0.26 | 10.1 |
| Rpl7a | 0.25 | 40.9 |
| RplP0 | 0.20 | -4.0 |

**Translation factors**

| Name | %mass | Net charge |
|---|---|---|
| Eef1a1 | 2.7 | 11.4 |
| Eef2 | 1.1 | -4.8 |
| Eif5a | 0.50 | -7.1 |
| Eef1d | 0.39 | -14.8 |

**Others**

| Name | %mass | Net charge |
|---|---|---|
| Mif | 1.9 | 0.8 |
| LgaLs1 | 0.79 | -3.4 |
| Tkt | 0.47 | 1.7 |
| Cltc | 0.38 | -39.8 |
| GstP1 | 0.33 | -3.3 |
| Eif4a1 | 0.26 | -9.0 |
| FasN | 0.23 | -34.1 |

## References


Bancaud, A., Huet, S., Daigle, N., Mozziconacci, J., Beaudouin, J. and Ellenberg, J., 2009. "Molecular crowding affects diffusion and binding of nuclear proteins in heterochromatin and reveals the fractal organization of chromatin." *EMBO J.*, **28**: 3785-3798.

Baum, M., Erdel, F., Wachsmuth, M. and Rippe, K., 2014. "Retrieving the intracellular topology from multi-scale protein mobility mapping in living cells." *Nat. Commun.*, **5**: 4494.

Betzig, E., Patterson, G. H., Sougrat, R., Lindwasser, O. W., Olenych, S., Bonifacino, J. S., Davidson, M. W., Lippincott-Schwartz, J. and Hess, H. F., 2006. "Imaging intracellular fluorescent proteins at nanometer resolution." *Science*, **313**: 1642-1645.

Boersma, A. J., Zuhorn, I. S. and Poolman, B., 2015. "A sensor for quantification of macromolecular crowding in living cells." *Nat. Methods*, **12**: 227-229.

Boisvert, F. M., van Koningsbruggen, S., Navascues, J. and Lamond, A. I., 2007. "The multifunctional nucleolus." *Nat. Rev. Mol. Cell Biol.*, **8**: 574-585.

Cognet, L., Leduc, C. and Lounis, B., 2014. "Advances in live-cell single-particle tracking and dynamic super-resolution imaging." *Curr. Opin. Chem. Biol.*, **20**: 78-85.

Cremer, T. and Cremer, C., 2001. "Chromosome territories, nuclear architecture and gene regulation in mammalian cells." *Nat. Rev. Genet.*, **2**: 292-301.

Digman, M. A. and Gratton, E., 2011. "Lessons in fluctuation correlation spectroscopy." *Annu. Rev. Phys. Chem.*, **62**: 645-668.

Dross, N., Spriet, C., Zwerger, M., Muller, G., Waldeck, W. and Langowski, J., 2009. "Mapping eGFP oligomer mobility in living cell nuclei." *PLoS One*, **4**: e5041.

Ebbinghaus, S., Dhar, A., McDonald, D. and Gruebele, M., 2010. "Protein folding stability and dynamics imaged in a living cell." *Nat. Methods*, **7**: 319-323.

Elf, J. and Barkefors, I., 2019. "Single-molecule kinetics in living cells." *Annu. Rev. Biochem.*, **88**: DOI:10.1146/annurev-biochem-013118-110801.

Elf, J., Li, G. W. and Xie, X. S., 2007. "Probing transcription factor dynamics at the single-molecule level in a living cell." *Science*, **316**: 1191-1194.

Enderlein, J., Gregor, I., Patra, D., Dertinger, T. and Kaupp, U. B., 2005. "Performance of fluorescence correlation spectroscopy for measuring diffusion and concentration." *ChemPhysChem*, **6**: 2324-2336.

English, B. P., Hauryliuk, V., Sanamrad, A., Tankov, S., Dekker, N. H. and Elf, J., 2011. "Single-molecule investigations of the stringent response machinery in living bacterial cells." *Proc. Natl. Acad. Sci. U. S. A.*, **108**: E365-E373.

Gitlin, I., Carbeck, J. D. and Whitesides, G. M., 2006. "Why are proteins charged? Networks of charge-charge interactions in proteins measured by charge ladders and capillary electrophoresis." *Angew. Chem.-Int. Edit.*, **45**: 3022-3060.

Ishikawa-Ankerhold, H. C., Ankerhold, R. and Drummen, G. P. C., 2012. "Advanced fluorescence microscopy techniques-FRAP, FLIP, FLAP, FRET and FLIM." *Molecules*, **17**: 4047-4132.

Knight, A. M., Culviner, P. H., Kurt-Yilmaz, N., Zou, T. S., Ozkan, S. B. and Cavagnero, S., 2013. "Electrostatic effect of the ribosomal surface on nascent polypeptide dynamics." *ACS Chem. Biol.*, **8**: 1195-1204.

Kusumi, A., Tsunoyama, T. A., Hirosawa, K. M., Kasai, R. S. and Fujiwara, T. K., 2014. "Tracking single molecules at work in living cells." *Nat. Chem. Biol.*, **10**: 524-532.

Liebermeister, W., Noor, E., Flamholz, A., Davidi, D., Bernhardt, J. and Milo, R., 2014. "Visual account of protein investment in cellular functions." *Proc. Natl. Acad. Sci. U. S. A.*, **111**: 8488-8493.

Lippincott-Schwartz, J., Snapp, E. and Kenworthy, A., 2001. "Studying protein dynamics in living cells." *Nat. Rev. Mol. Cell Biol.*, **2**: 444-456.

Lodish, H., Berk, A., Matsudaira, P., Kaiser, C. A., Krieger, M., Scott, M. P., Zipursky, L. and Darnell, J. (2003). Molecular Cell Biology. New York, W.H. Freeman**:** 253.

Machan, R. and Wohland, T., 2014. "Recent applications of fluorescence correlation spectroscopy in live systems." *FEBS Lett.*, **588**: 3571-3584.

Manley, S., Gillette, J. M., Patterson, G. H., Shroff, H., Hess, H. F., Betzig, E. and Lippincott-Schwartz, J., 2008. "High-density mapping of single-molecule trajectories with photoactivated localization microscopy." *Nat. Methods*, **5**: 155-157.

Manzo, C. and Garcia-Parajo, M. F., 2015. "A review of progress in single particle tracking: from methods to biophysical insights." *Rep. Prog. Phys.*, **78**: 124601.

Milo, R. and Phillips, R. (2016). Cell Biology by the Numbers. New York, NY, Garland Science.

Mu, X., Choi, S., Lang, L., Mowray, D., Dokholyan, N. V., Danielsson, J. and Oliveberg, M., 2017. "Physicochemical code for quinary protein interactions in *Escherichia coli*." *Proc. Natl. Acad. Sci. U. S. A.*, **114**: E4556-E4563.

Potma, E. O., de Boeij, W. P., Bosgraaf, L., Roelofs, J., van Haastert, P. J. M. and Wiersma, D. A., 2001. "Reduced protein diffusion rate by cytoskeleton in vegetative and polarized Dictyostelium cells." *Biophys. J.*, **81**: 2010-2019.

Ries, J. and Schwille, P., 2012. "Fluorescence correlation spectroscopy." *Bioessays*, **34**: 361-368.

Rivas, G. and Minton, A. P., 2016. "Macromolecular crowding *in vitro*, *in vivo*, and in between." *Trends Biochem.Sci.*, **41**: 970-981.

Rust, M. J., Bates, M. and Zhuang, X., 2006. "Sub-diffraction-limit imaging by stochastic optical reconstruction microscopy (STORM)." *Nat. Methods*, **3**: 793-795.

Schavemaker, P. E., Smigiel, W. M. and Poolman, B., 2017. "Ribosome surface properties may impose limits on the nature of the cytoplasmic proteome." *eLife*, **6**: e30084.

Schwartz, R., Ting, C. S. and King, J., 2001. "Whole proteome pI values correlate with subcellular localizations of proteins for organisms within the three domains of life." *Genome Res.*, **11**: 703-709.

Seksek, O., Biwersi, J. and Verkman, A. S., 1997. "Translational diffusion of macromolecule-sized solutes in cytoplasm and nucleus." *J. Cell Biol.*, **138**: 131-142.

Smith, A. E., Zhou, L. Z., Gorensek, A. H., Senske, M. and Pielak, G. J., 2016. "In-cell thermodynamics and a new role for protein surfaces." *Proc. Natl. Acad. Sci. U. S. A.*, **113**: 1725-1730.

Tojkander, S., Gateva, G. and Lappalainen, P., 2012. "Actin stress fibers - assembly, dynamics and biological roles." *J. Cell Sci.*, **125**: 1855-1864.

Wirth, A. J. and Gruebele, M., 2013. "Quinary protein structure and the consequences of crowding in living cells: Leaving the test-tube behind." *Bioessays*, **35**: 984-993.

Yan, R., Moon, S., Kenny, S. J. and Xu, K., 2018. "Spectrally resolved and functional super-resolution microscopy via ultrahigh-throughput single-molecule spectroscopy." *Acc. Chem. Res.*, **51**: 697-705.

Yang, Z. G., Cao, J. F., He, Y. X., Yang, J. H., Kim, T., Peng, X. J. and Kim, J. S., 2014. "Macro-/micro-environment-sensitive chemosensing and biological imaging." *Chem. Soc. Rev.*, **43**: 4563-4601.

Zhang, M. S., Chang, H., Zhang, Y. D., Yu, J. W., Wu, L. J., Ji, W., Chen, J. J., Liu, B., Lu, J. Z., Liu, Y. F., Zhang, J. L., Xu, P. Y. and Xu, T., 2012. "Rational design of true monomeric and bright photoactivatable fluorescent proteins." *Nat. Methods*, **9**: 727-729.